ELSEVIER

Journal of Molecular Catalysis A: Chemical 168 (2001) 265–277

JOURNAL OF MOLECULAR CATALYSIS A: CHEMICAL

www.elsevier.com/locate/molcata

Parametric calculations of Mo-allyl complexes anchored on silica

Beulah Griffe [a,*], Anibal Sierraalta [b], Fernando Ruette [b], Joaquín L. Brito [a]

[a] *Laboratorios de Síntesis y Caracterización de Nuevos Materiales, Centro de Química, Instituto Venezolano de Investigaciones Científicas, I.V.I.C., Apartado 21827, Caracas 1020-A, Venezuela*

[b] *y Química Computacional, Centro de Química, Instituto Venezolano de Investigaciones Científicas, I.V.I.C., Apartado 21827, Caracas 1020-A, Venezuela*

Received 10 May 2000; received in revised form 11 September 2000; accepted 7 November 2000

Abstract

The SiO_2 anchored $Mo(\eta^3\text{-}C_3H_5)_4$ catalyst was modeled by means of the CNDO-UHF parametrical method. Two models (two separated centers (TSC) and two adjacent centers (TAC)) were proposed for the silica pre-treated at relatively low temperature. An analysis of total energies, bond indexes, diatomic energies, and parametric diatomic binding energies for selected bonds suggests the existence of both models on the surface. However, TSC is favored with respect to TAC. Furthermore, it is observed an allyl group interaction with the support through a C–O bond that leads to a C–C bond activation. Also, C–H activation is found due to Mo–H interaction. These results support several features of the generally accepted mechanism for olefin metathesis in this type of catalyst. Finally, experimental results of NMR, obtained in previous work by some of the authors, are interpreted by inequivalency of different allyl ligands. © 2001 Elsevier Science B.V. All rights reserved.

Keywords: Parametric method; Metathesis; Mo-allyl catalyst; CNDO-UHF; Anchored complex

1. Introduction

Conventional preparation methods of heterogeneous catalysts normally involve the use of inorganic compounds of the elements of interest. Organometallic complexes, especially those of the transition metals, have been employed in the last three decades in an attempt to synthesize better defined solids [1]. The basic underlying concept is that part of complex ligands can be substituted by the surface functionalities of the supports. Thus, molecularly well-defined surface species that are anchored onto the support exhibit properties of both heterogeneous and homogeneous catalysts. So, in an organometallic sense, the supported metallic species become *ligands* of the surface [2].

Molybdenum based catalysts are employed in a variety of catalytic reactions of both industrial and laboratory interest. Catalytic reactions of these materials range from reducing transformations (hydrogenation or hydrogenolysis) to partial or complete oxidation and disproportionation reactions [3]. Such versatility is possible due to the existence of several stable oxidation states of the Mo centers, and because this element can form species of diverse nuclearity by varying the conditions chosen for the synthesis, pre-treatment and/or reaction.

Molybdenum allylic and carbonylic complexes and in some cases the chlorides have all been employed for the synthesis of catalysts by grafting techniques. These complexes react protolytically with acidic OH groups of the surfaces of silica, alumina, etc. rendering a fragment of the cluster fixed through the oxygen atom to the surface. The proton is released with the

* Corresponding author.

1381-1169/01/$ – see front matter © 2001 Elsevier Science B.V. All rights reserved.
PII: S1381-1169(00)00543-4

ligand liberated by the reaction, forming, e.g. propene, HCl, or molecular H_2 plus CO [4,5]. The allyl group is a particularly good leaving ligand during both the fixation of the complex to the surface and the latter modification of the local environment around the Mo centers induced by treatments such as reduction, oxidation, sulfiding, etc.

Yermakov et al. were the first authors to report studies of Mo(η^3-C_3H_5)$_4$ on silica and alumina [6,7]. Afterwards, Iwasawa's group also reported work on catalysts derived from Mo(η^3-C_3H_5)$_4$ and from the dimer Mo_2(η^3-C_3H_5)$_4$ [8,9]. The Japanese workers thoroughly characterized the supported systems (typical Mo loading ca. 2 wt.%) by means of an array of techniques, including among others UV–VIS and IR spectroscopy, EXAFS, XPS, temperature-programmed decomposition and catalytic transformations such as olefin metathesis, alcohol oxidation, etc. The results suggested that the surface bound allylic species were uniformly distributed on the support surfaces. However, most of these characterization studies were performed on the allyl-derived catalysts after reduction–oxidation transformations. In fact, most research on Mo-allyl supported catalysts characterization has been carried out after organic ligands release induced by reduction–oxidation pre-treatments. However, the anchored organometallic species have not received comparable attention, contrary to the case of similar surface species of other transition metals (e.g. Rh, Sn) [2].

Published results on the supported Mo-allyl system are limited so far to some IR spectra by Yermakov [6,7], PAS/FTIR by McKenna and Eyring [10], stoichiometric measurements of the surface reaction by Yu [11] and XPS by Aigler et al. [12]. Some of us have recently studied the SiO_2 attached monomeric and dimeric Mo-allyl complexes using PAS-FTIR and solid state ^{1}H and ^{13}C-NMR, without any further reduction–oxidation pre-treatment, in order to characterize the surface allylic species [13]. PAS-FTIR of the monomeric species showed, besides the characteristic C–H bands, two additional signals at 1700 and 1470 cm^{-1}, assigned to the stretching of C=C bonds in η^1- and η^3-allylic species, respectively [10,13]. In ^{1}H MAS-NMR [13–15] five signals were observed, corroborating the presence of both η^3- and η^1-allylic species in the SiO_2-attached Mo-allyl catalyst. Velásquez [14], found at least four signals employing ^{13}C-NMR CP-MAS, which were interpreted as due to a mixture of η^3- and η^1-coordinated allylic species. Nevertheless, one of the expected signals at 120 ppm, for the η^1 co-ordination was not clearly observed.

The objective of this work is to model a Mo-allyl fragment anchored on silica (Mo(η^3-C_3H_5)$_2$–silica), a catalyst that has been previously used as olefin metathesis catalyst. The starting Mo-allyl complex was Mo(η^3-C_3H_5)$_4$ and the support surface was simulated by a β-crystobalite cluster ($Si_8O_{24}H_{16}$). The method employed is a modified version of the parametrical method CNDO [16]. Calculation of bonding properties are used to understand the possible structure of the immobilized complex and feasible mechanisms in the metathesis reaction of propene. Bonds development between anchored complex and the support, and bond activation would suggest the presence of possible intermediates and transition state structures.

2. Computational and theoretical details

The theoretical method employed was a parametric method based on CNDO-UHF [16] from GEOMO program [17] with several modifications [18,19] that include also the calculation of diatomic binding energies and Mulliken population with non-orthogonal orbitals. The atomic set of parameters is presented in a previous work [20]. Here, however, new molecular parameters are introduced in order to improve the calculation of total and diatomic binding energies.

It is well known that CNDO significantly overestimates binding energies [21–25]. To overcome this methodological difficulty, a new simple parametrization procedure is introduced, which allows obtaining more reasonable total binding energies (TBE) values. This approach is based on the partition of TBE [19] and the total energy E_T [26–28]. Thus, the TBE can be calculated in terms of diatomic binding energies (DBEs) [29] for all A–B bonds in the molecular system

$$\mathrm{TBE} = \sum_{B>A} \mathrm{DBE(A\text{–}B)} = E_T - \sum_{A} \varepsilon_A^0 \qquad (1)$$

where ε_A^0 terms correspond to energies of free A atoms. However, as mentioned above, DBEs can be parametrized (PDBEs) as follows:

$$\mathrm{PDBE(A\text{–}B)} = \alpha_{AB}\mathrm{DBE(A\text{–}B)} \qquad (2)$$

The α_{AB} parameters were obtained from the relation between experimental values of dissociation energy for bonds (DEB) and their respective calculated DBEs; i.e. α_{AB} = DEB(A–B)/DBE(A–B) is a fixed parameter for all systems that contain the A–B bond.

DEBs were taken as follows: Mo–C from $Mo(CO)_6$ [30]; C–O, C–H, O–H, from average values [31]; Mo–H [32], and Mo–O, Si–O, C–C, and H–H from values of the diatomic molecules [33]. Because experimental or theoretical data for MoSi has been not reported, calculations with DFT using UB3LYP/LANL2DZ in the Gaussian-94 program [34] were carried out. The binding energy of $-28.41\,\text{kcal mol}^{-1}$ and a distance of 2.6467 Å were attained. The most stable multiplicity of 7 was obtained, for a state in which orbital symmetries were broken. These calculated parameter values of α_{AB}, for the most important interacting atoms were H–H = 0.95; C–H = 0.43; O–H = 0.65; C–C = 0.27; C–O = 0.29; Si–O = 1.07; Mo–O = 0.64; Mo–Si = 0.10; Mo–H = 0.62; and Mo–C = 0.16.

The parametrized total energy (E_{TP}) can be calculated in terms of PDBEs using Eq. (1)

$$E_{TP} = \sum_{A} \varepsilon_A^0 + \sum_{B>A} \text{PDBE(A–B)}. \tag{3}$$

Chemisorption energy (CE) can be evaluated as the sum of PDBE between fixed fragment (A_i) and surface (S_κ) atoms (A–S bonds), and PDBE changes of the interacting atoms on the fixed fragment and the substrate with respect to the correspondent isolated systems. Thus,

$$\text{CE} = \sum_{i,\kappa}^{\text{NAS}} \text{PDBE}(A_i\text{–}S_\kappa) + \sum_{i,j}^{\text{NA}} \Delta\text{PDBE}(A_i\text{–}A_j) + \sum_{\kappa,\lambda}^{\text{NS}} \Delta\text{PDBE}(S_\kappa\text{–}S_\lambda) \tag{4}$$

where NAS are the number of interacting atom pairs between fragment and surface. NA and NS are those that have a significant change in their bonds in A and in S, respectively.

In the case of charge density calculations, the population analysis is evaluated in an approximated way using the Mulliken approximation [35]

$$N = \sum_{\mu v} P_{\mu v} S_{\mu v} \tag{5}$$

where N is the total number of electrons. $P_{\mu v}$ and $S_{\mu v}$ correspond to the density matrix and overlap matrix components, respectively. Note that this is an approximated population, because the basis set used in obtaining $P_{\mu v}$ is implicitly included in parametric functionals. It does not necessarily correspond to that used in $S_{\mu v}$ calculations [36,37]. Normally, in parametric methods, the atomic orbitals are assumed orthogonalized by a transformation that is unknown. In this work, the symmetric transformation [38] was selected, because it maintains the correct Fock matrix symmetry. Therefore, the calculated orbitals are deorthogonalized and the standard population analysis is applied according to Eq. (5).

3. Modeled surface species

It is well known that partially hydroxilated silica is amorphous. Nevertheless, previous evidences suggest a structure similar to β-crystobalite and related crystalline phases [39]. The degree of hydroxylation of the silica is a function of the pre-treatment temperature [40]. In previous experimental studies [15], the silica was pre-treated at 150–750°C. At the highest temperature, mainly free (isolated) OH groups are retained at the surface of this support [41]. At lower temperatures, there is a probability of finding geminal and bridge OH groups. Due to these facts, a cluster of silica of formula $Si_8O_{24}H_{16}$, with both isolated and geminal OH groups and a structure similar to the (1 1 1) face of β-crystobalite [39], was selected as a model of the support. The cluster with its anchoring sites is shown in Fig. 1. Note that all O edge atoms are saturated with H.

The reaction of the $Mo(\eta^3\text{-}C_3H_5)_4$ complex (see Fig. 2) with the surface of hydroxilated supports has been shown to proceed by protolysis of the OH groups and fixing of the organometallic fragment to the surface, as indicated in Scheme 1. Iwasawa, by means of TPD [9] and Yermakov and Zakharov [6,7], employing GC and mass spectroscopy, have verified the suggested stoichiometry of this reaction.

In order to model this interaction, a fragment consisting of the Mo center and two allyl ligands

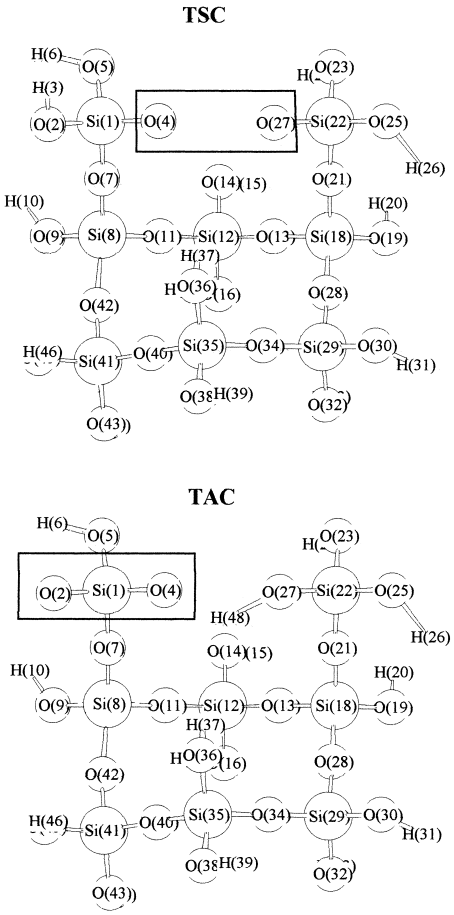

Fig. 1. $Si_8O_{24}H_{16}$ cluster with anchored sites located on: (a) oxygen atoms bonded to two different Si atoms (two separated centers (TSC)); (b) oxygen atoms bonded to the same Si atom (two adjacent centers (TAC)).

$Mo(\eta^3\text{-}C_3H_5)_2$ was attached to O_4 and O_{27} oxygens (shown in Fig. 3). These two oxygens were chosen since the distance between them in the $Si_8O_{24}H_{16}$ cluster is 2.80 Å, which can be optimal for O–Mo–O interactions. The immobilized fragment and the support resulted in a 63-atom cluster, as can be appreciated in Fig. 3. This will be called the "two-separated-centers" model (TSC).

A model in which the monomer reacts with two OH groups in the same tetrahedral unit of the silica support was also considered, as shown in Scheme 2.

This situation is possible in some experimental conditions [15]. Mo-allyl catalysts preparations have sometimes been made with supports pre-treated at relatively low temperatures that allow the presence of such geminal hydroxyls [41]. The corresponding structure is shown in Fig. 4, and it will be called the "two-adjacent-centers" model (TAC).

4. Results and discussion

In first place, calculated properties of the $Mo(\eta^3\text{-}C_3H_5)_4$ molecule were analyzed. The optimized structure revealed a distorted tetrahedral symmetry, even in the case in which equal Mo–C distances (about 2.30 Å) were used as starting point for optimization. This starting distance value was selected from experimental data [42]. The distortion can be appreciated in Fig. 2 after optimization of all the allyl angles. This result is in agreement with ^1H solution NMR results by Ramey et al. [43] that prove an inequivalency of different allyl protons of this complex.

In addition, with the purpose of comparing results, calculations were also carried out for the isolated amorphous hydroxilated silica ($Si_8O_{24}H_{16}$), starting with the experimental geometry data [44]. The theoretically calculated Si–O average bond distance (1.65 Å) compares well with other theoretical calculations at HF and DFT (1.61–1.66 Å) [45,46] and with the experimental values of 1.61 Å [44]. The calculated Si–Si distance was about 3.32 Å which is close to the experimental value of 3.10 Å [32] and other theoretical results 3.23–3.40 Å [45]. The average charge values ($q(O) = -0.71$, $q(Si) = +1.90$) are smaller than those reported at ab initio level [45] ($q(O) = -1.02$ to -1.17, $q(Si) = 2.32$ to 2.34).

With the purpose of studying the formation and structure of the anchored complex with η^3 coordination, calculations of $Mo(\eta^3\text{-}C_3H_5)_2/Si_8O_{24}H_{14}$ were carried out. The geometry of the substrate was maintained fixed, except for the Si–O bond of the anchoring site The $Mo(\eta^3\text{-}C_3H_5)_2$ fragment was attached to the immobilizing sites at the optimal Mo–O distances of 2.10 and 1.98 Å for TSC and 2.18 and 2.10 Å for TAC and then an optimization of the ligand angles was performed.

4.1. TSC model

In order to analyze the anchored fragment interaction and the adsorption effect on the support, results

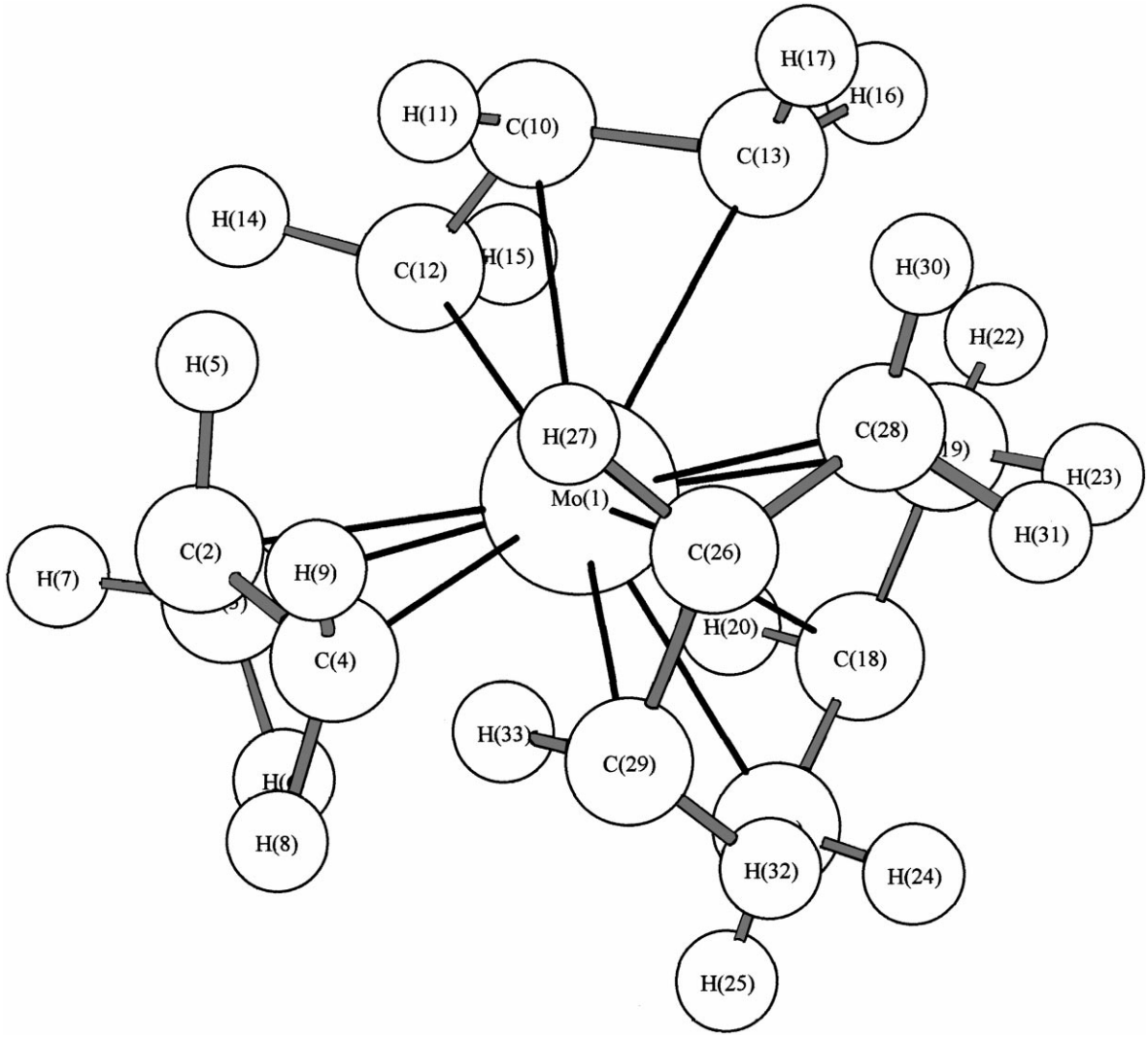

Fig. 2. $Mo(\eta^3\text{-}C_3H_5)_4$ complex.

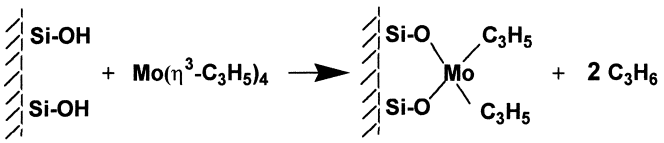

(I)

Scheme 1.

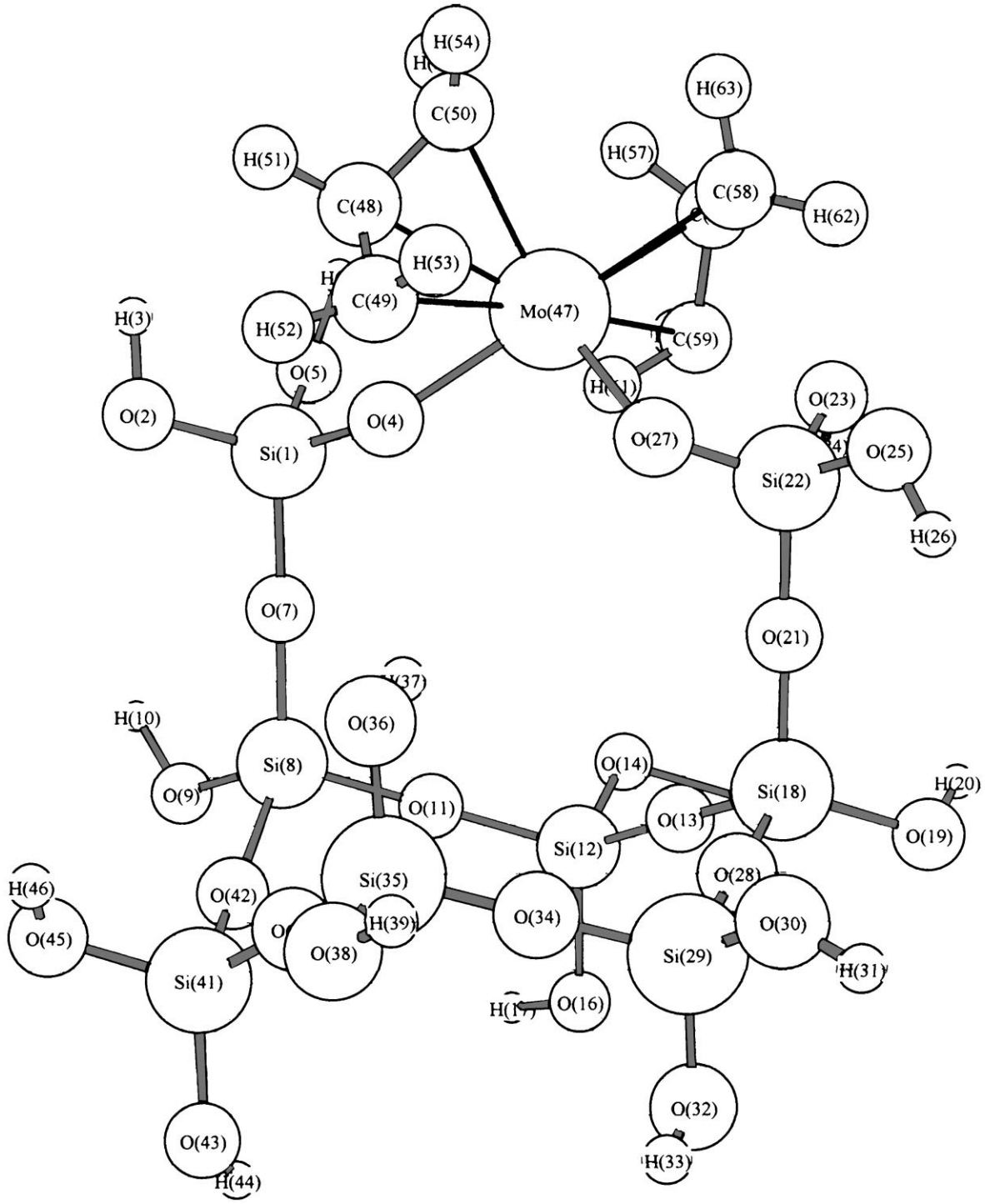

Fig. 3. Anchored $Mo(\eta^3\text{-}C_3H_5)_2$ fragment on $Si_8O_{24}H_{14}$. The TSC model.

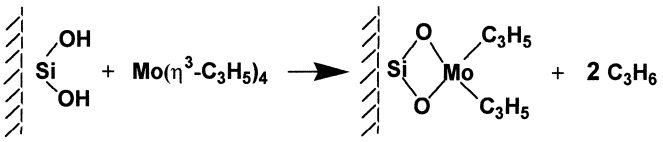

(II)

Scheme 2.

of Wiberg's indexes (WI), diatomic energies (DE), and parametrized diatomic binding energies (PDBEs) for selected Mo–O, Mo–Si, Mo–C, Mo–H, C–H, C–C, C–O, and Si–O bonds were calculated. The value of these variables, for TSC model, are presented in Table 1. Values in parentheses correspond to the non-interacting systems.

Several features can be drawn from the analysis of bonding changes due to the interactions with the modeled silica surface:

1. The feasibility of the fixed fragment was evaluated as the total energy difference (ΔE_T) between products and reactants of ($\Delta E_T = -185.6\,\text{kcal mol}^{-1}$)

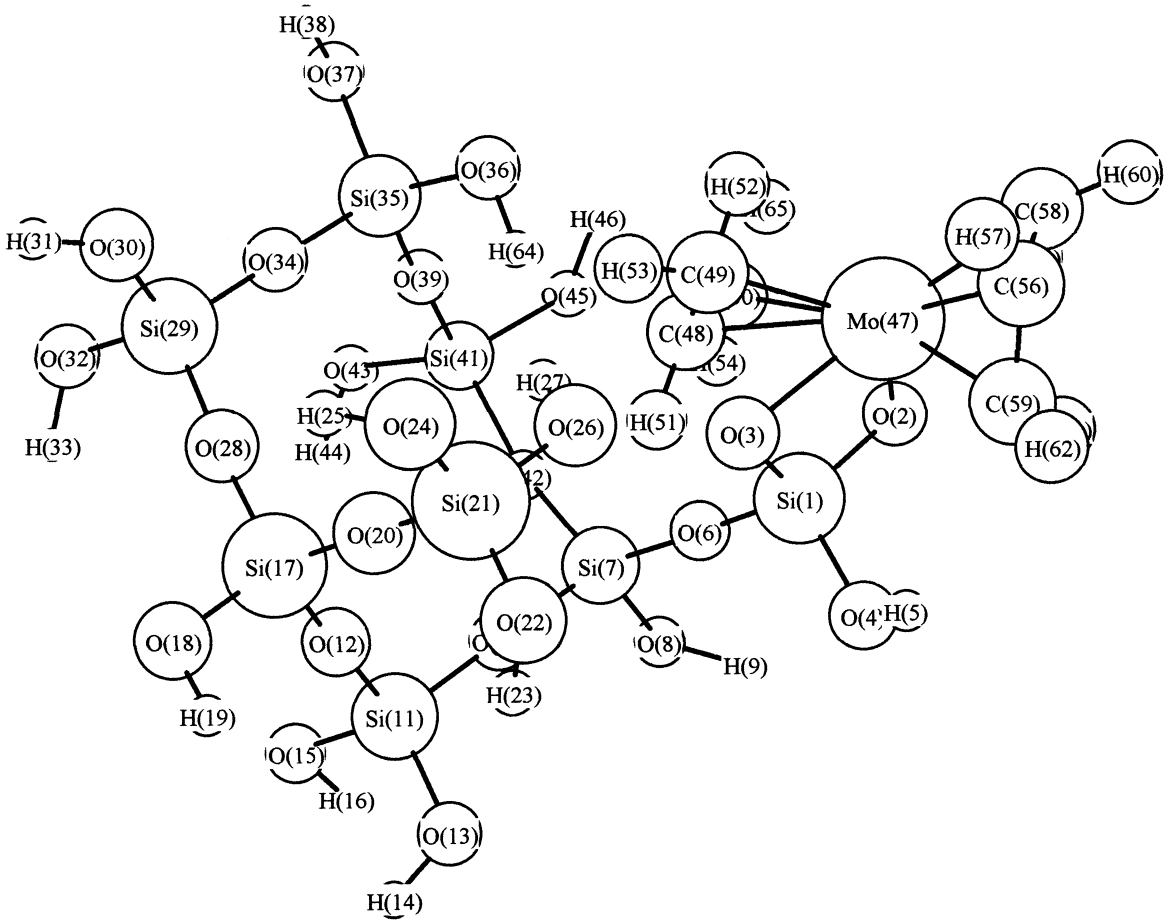

Fig. 4. Anchored $Mo(\eta^3\text{-}C_3H_5)_2$ fragment on TSC of $Si_8O_{24}H_{14}$. The TAC model.

Table 1
Selected Wiberg indexes (WI), diatomic energies (DE), and parametrized diatomic binding energies (PDBE) for the immobilized $Mo(\eta^3\text{-}C_3H_5)_2$ on $Si_8O_{24}H_{14}$[a]

Bond	WI	DE (a.u.)	PDBE (kcal mol^{-1})
Si_1–O_2	1.310 (1.281)[b]	−0.841 (−0.821)	−150.17 (−141.51)
Si_1–O_4	0.915 (1.364)	−0.684 (−0.906)	−130.64 (−141.78)
Si_1–O_5	1.269 (1.255)	−0.841 (−0.834)	−151.47 (−148.14)
Si_1–O_7	1.349 (1.248)	−0.906 (−0.855)	−126.21 (−115.25)
Si_{22}–O_{21}	1.221 (1.267)	−0.839 (−0.870)	−126.97 (−118.93)
Si_{22}–O_{23}	1.157 (1.294)	−0.756 (−0.849)	−142.83 (−150.98)
Si_{22}–O_{25}	1.247 (1.268)	−0.821 (−0.836)	−160.76 (−150.38)
Si_{22}–O_{27}	1.137 (1.223)	−0.754 (−0.803)	−118.71 (−149.56)
Mo_{47}–O_4	0.410	−0.281	−53.15
Mo_{47}–O_{27}	0.989	−0.544	−87.05
Mo_{47}–Si_1	0.104	−0.196	−6.85
Mo_{47}–C_{48}	0.350 (0.441)	−0.305 (−0.332)	−18.44 (−20.02)
Mo_{47}–C_{50}	0.408 (0.306)	−0.364 (−0.374)	−21.36 (−21.89)
Mo_{47}–C_{49}	0.155 (0.494)	−0.231 (−0.436)	−13.84 (−25.39)
Mo_{47}–C_{56}	0.272 (0.387)	−0.301 (−0.320)	−18.19 (−19.31)
Mo_{47}–C_{58}	0.618 (0.537)	−0.426 (−0.396)	−25.03 (−23.02)
Mo_{47}–C_{59}	0.629 (0.452)	−0.428 (−0.342)	−25.09 (−20.23)
C_{49}–O_4	0.896	−0.957	−72.70
C_{48}–C_{50}	1.615 (1.121)	−1.440 (−1.235)	−112.78 (−94.17)
C_{48}–C_{49}	1.027 (1.400)	−1.110 (−1.340)	−89.60 (−104.89)
Mo_{47}–H_{61}	0.051 (0.027)	−0.061 (−0.022)	−22.43 (−8.03)
C_{58}–H_{61}	0.896 (0.937)	−0.713 (−0.732)	−65.09 (−91.67)

[a] The TSC model.
[b] Values in parentheses correspond to isolated systems ($Si_8O_{24}H_{16}$ and $Mo(C_3H_5)_4$).

$$\underset{-185.6}{\Delta E_T(\text{kcalmol}^{-1})} = \underset{(-7142.1)}{E_T(\text{fragment-silica})} + 2\underset{(-1585.0)}{E_T(\text{propene})} - \underset{(-2995.7)}{E_T(\text{complex})} - \underset{(-5545.8)}{E_T(\text{silica})}$$

2. PDBEs values for Si–O in the isolated system are in the range of −115 to −151 kcal mol^{-1} being, as expected, smaller than the Si–O bond strength (−188 kcal mol^{-1}) in the diatomic molecule [32]. In general, there is a good correlation between WIs, DEs, and PDBEs; i.e. an increase or decrease of the bond strength in the anchored compound or the modeled surface with respect to the corresponding free systems is reflected in all of these variables. It is observed that Mo–O bonding (Mo–O_4 and Mo–O_{27}) interactions lead to a weakening of surface Si–O bonds (Si_1–O_4 and Si_{22}–O_{27}) that directly interact with Mo. This is reflected in longer Si–O bond distances (about 1.89 Å) than in the isolated cluster (1.66 Å). However, some internal Si–O bonds are strengthened (Si_1–O_2, Si_1–O_7). Note that every tool used to analyze bond strength takes more into account some bond features that others do not consider. For example, WIs are involved mainly with covalent bond contributions; DEs comprise both components: ionic and covalent; and PDBEs include, beside these components, changes in the atomic energy due to the bonding interactions [19].
3. Interaction of Mo with O surface atoms is not symmetric, therefore, the $Mo(C_3H_5)_2$ fragment is tilted on the surface, as shown in Fig. 3. Bonding of Mo–O_{27} is stronger than that of Mo–O_4, as shown in Table 1, and the corresponding bond distance of the former (1.97 Å) is shorter than the Mo–O_4 one (2.10 Å). This fact can be explained by an allyl (C_{49}–C_{48}–C_{50}) interaction with the support through a C_{49}–O_4 bonding (−59.6 kcal mol^{-1}, see Fig. 3) at a distance of 1.56 Å. This seems to suggest a partial co-ordination of at least one allyl ligands with the support is feasible. The other allyl (C_{56}–C_{58}–C_{59}) does not interact directly with the SiO_2 cluster, and it corresponds to an standard η^3-coordination with Mo. For that reason, it

is also observed in Table 1 that the Mo–C bonds become more asymmetric after the anchoring process. Therefore, some of the allyl carbon atoms are more tightly bonded to Mo than others are. These theoretical results may, in part, provide an explanation for spectroscopic experimental results [14,15] in which apparently both η^3 and η^1 types of co-ordination were identified by ^{1}H MAS-RMN and PAS-FTIR, however, only four signals of five were clearly observed in the ^{1}H MAS-RMN spectrum. That is, according to the calculations, one of the ligand possesses a C–O interaction with the support. This fact could give a certain η^1-coordination character to this allyl bond to the Mo.

4. A comparison of the total Mo–C bond strength, in the free allyl complex (TPDBE(Mo–C) = $-129.9\,\text{kcal mol}^{-1}$) with respect to Mo–O (TPDBE(Mo–O) = $-140.2\,\text{kcal mol}^{-1}$), suggests that the release of the allyl groups and formation of Mo–O bonds (and therefore, the Mo(η^3-C_3H_5)$_2$ fragment) are favored. That is, the complex prefers to replace two η^3-C_3H_5 ligands by a bidentate ligand located on the silica surface.
5. The reaction energy balance shown above indicates that the formation of the anchored complex is feasible. This result is in agreement with the CE value obtained from Eq. (4) for the bonds involved in the interaction. This is, the sum of broken, formed, strengthened, and weakened bonds produces a net energy stability. Thus, O–H scission on the surface and C–H formation in C_3H_6 produces a $-33.0\,\text{kcal mol}^{-1}$ of energy gaining. Energy stabilizations of $-56.9\,\text{kcal mol}^{-1}$ and -6.9 is obtained for the formation of C–O and Mo–Si bonds, respectively. The delta of energy for breaking Mo–C and forming Mo–O bonds is of $-10.3\,\text{kcal mol}^{-1}$. The sum of all H–Mo interactions yields $-44.2\,\text{kcal mol}^{-1}$. The C–C and C–H. bonds on allyl ligands are stabilized by -10.3 and destabilized by $20.5\,\text{kcal mol}^{-1}$, respectively. Mo–C bond changes give a destabilization of $7.9\,\text{kcal mol}^{-1}$. On other hand, C–C and C–H bonds in propane are stronger in $-71.5\,\text{kcal mol}^{-1}$ than those in the Mo(η^3-C_3H_5)$_4$ complex. Finally, Si–O bonds close to the Si atom bonded to the anchored site are destabilized ($31.7\,\text{kcal mol}^{-1}$). The sum yields a net energy gaining of $-173.0\,\text{kcal mol}^{-1}$ which is close to the value of $-185.6\,\text{kcal mol}^{-1}$ shown above. Note that this sum does not include small energy changes in other Si–O bonds.
6. An agostic $C_{58}\cdots H_{61}\cdots$Mo interaction is observed by the partial creation of Mo–H bond (PDBE(Mo–H_{61}) = $-14.6\,\text{kcal mol}^{-1}$ at 1.80 Å, see Fig. 5) and the weakening of C_{58}–H_{61} bond by $26.6\,\text{kcal mol}^{-1}$. These results are in agreement with the scheme of carbene (Mo–C (*n*-propenyl)) formation through a transition state in which a C–H bond is activated in the methylene group and a Mo–H bond is starting to be formed [47]. On the other hand, the C_{49}–O_4 interaction (see Fig. 5) produces in the other allyl group a weakening of C_{48}–C_{49} ($-18.61\,\text{kcal mol}^{-1}$) and a strengthening of C_{48}–C_{50} ($15.3\,\text{kcal mol}^{-1}$). This fact can be interpreted as an indication of carbene chain mechanism, via a metallacyclobutane intermediate, which is generally accepted for olefin metathesis [47]. The partial formation of Mo–H bond, the weakening of C–H and C–C bonds in the anchored Mo(η^3-C_3H_5)$_2$/SiO_2 could explain the high catalytic activity for olefin metathesis of the anchored Mo-allyl catalyst [47]. Because an allyl group can be bonded to the surface support, the formation of an active site available for olefine adsorption is favored. In addition, it is well known that the allyl group exhibits fluxional behavior. Therefore, η^3-allyl-metal group can be rearranged to a η^1-allyl-metal intermediate. Then, these two facts drive the approaching of bond activated allyl groups that lead to the formation of $C_2H_4 + C_4H_8$. In fact, butane and ethylene are among the products from the catalyst anchoring process [11].

4.2. TAC model

In the case of the TAC model interaction (see Fig. 4) similar features as in the TSC model, can be signaled (see Table 2). However, several important differences are observed

1. The total energy difference between products and reactants is $-144.5\,\text{kcal mol}^{-1}$ that is smaller than in the TSC case ($-185.6\,\text{kcal mol}^{-1}$). This trend is in agreement with interaction Mo–O for the TSC model being stronger (TDBE = $-140.2\,\text{kcal mol}^{-1}$) than for the TAC one (TDBE = $-114.7\,\text{kcal mol}^{-1}$).

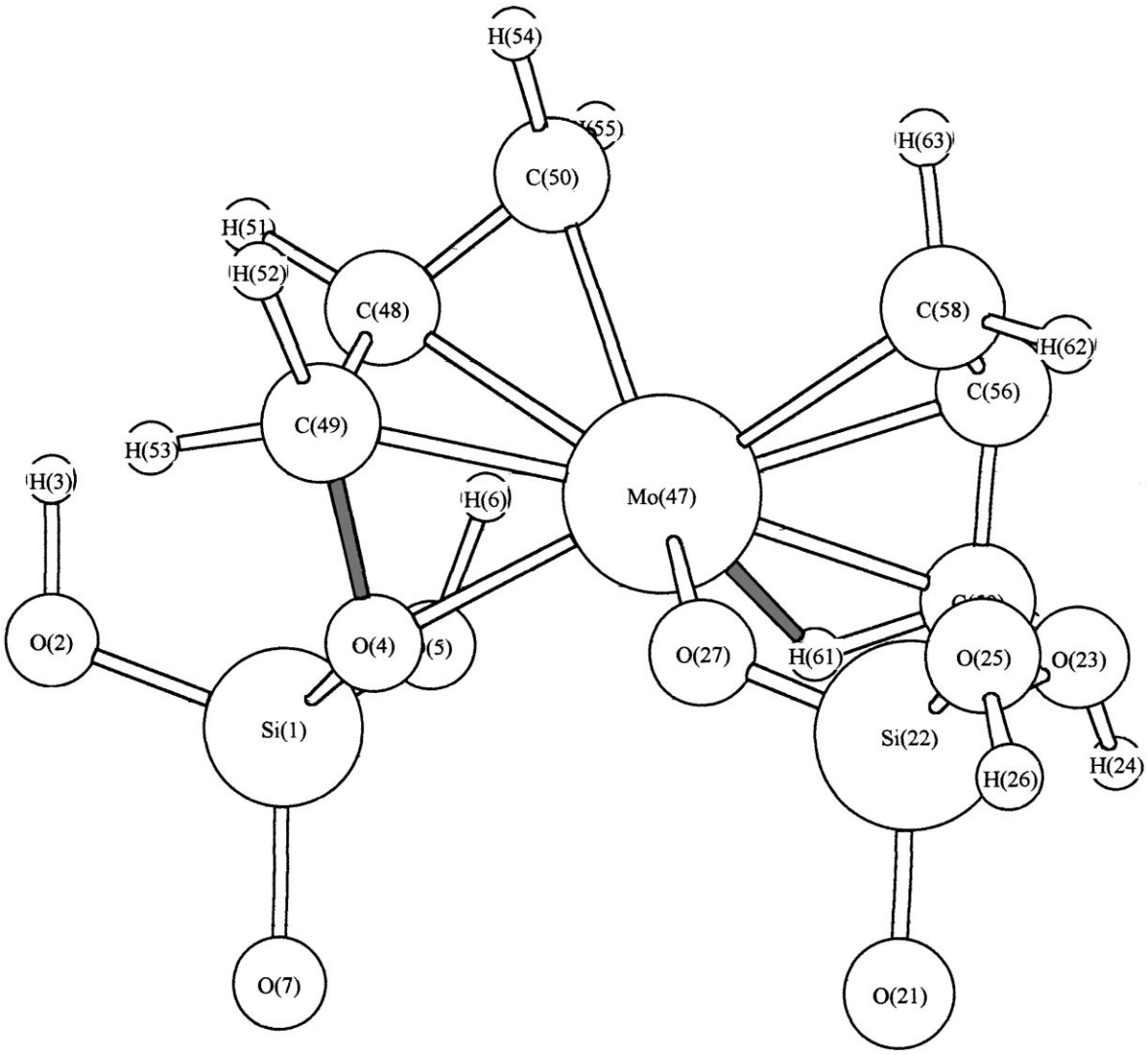

Fig. 5. C–O and Mo–H interactions in TSC model.

2. Mo–Si interaction is of greater magnitude ($-16.10\,\text{kcal mol}^{-1}$) than in the case of the TSC model ($-6.85\,\text{kcal mol}^{-1}$).
3. The energy changes of the surface Si–O bonds are stronger in the TAC model because the two oxygen atoms that interact with the Mo are bonded to the same Si atom.
4. The values of the binding energy (Mo–O_3 and Mo–O_2), as well as in the above model, are not symmetric, in agreement with the fact that there is also a C_{48}–O_3 interaction of about -34.3 kcal mol^{-1}, as shown in Table 2. As in the TSC model, this interaction could also explain the mechanism of activation of C–C bond (18.0 kcal mol^{-1}) for the formation of a metallacyclobutane intermediate.
5. The partial formation of an agostic C–H–Mo bond (C–H activation) is clearer in TAC than in TSC model. The PDBEs for TAC (-65.1 and -30.1 kcal mol^{-1} for C_{58}–H_{61} and Mo–H_{61}, respectively) are weaker and stronger than those of TSC (-85.3 and $-14.6\,\text{kcal mol}^{-1}$ for C_{58}–H_{61} and Mo–H_{61}, respectively). Therefore, hydrogen transfer with

Table 2
Selected Wiberg indexes (WI), diatomic energies (DE) and parametrized diatomic binding energies (PDBE) for the immobilized $Mo(C_3H_5)_2$ on $Si_8O_{24}H_{16}$[a]

Bond	WI	DE (a.u.)	PDBE (kcal mol^{-1})
Si_1–O_2	1.972 (1.281)[b]	−0.688 (−0.821)	−114.44 (−141.51)
Si_1–O_3	0.847 (1.364)	−0.609 (−0.900)	−126.58 (−141.78)
Si_1–O_4	1.302 (1.255)	−0.842 (−0.834)	−165.85 (−148.14)
Si_1–O_6	1.276 (1.248)	−0.870 (−0.855)	−134.29 (−115.25)
Mo_{47}–O_2	0.729	−0.438	−66.84
Mo_{47}–O_3	0.523	−0.270	−47.85
Mo_{47}–Si_1	0.478	−0.464	−16.10
Mo_{47}–C_{48}	0.156 (0.491)	−0.219 (−0.332)	−12.63 (−20.02)
Mo_{47}–C_{49}	0.887 (0.494)	−0.475 (−0.436)	−26.11 (−25.39)
Mo_{47}–C_{50}	0.789 (0.306)	−0.469 (−0.374)	−26.33 (−21.87)
Mo_{47}–C_{56}	0.314 (0.387)	−0.292 (−0.320)	−16.78 (−19.31)
Mo_{47}–C_{58}	0.746 (0.537)	−0.453 (−0.396)	−25.31 (−23.02)
Mo_{47}–C_{59}	0.450 (0.452)	−0.441 (−0.342)	−24.66 (−20.23)
C_{48}–O_3	0.690	−0.807	−41.40
C_{48}–C_{50}	0.988 (1.121)	−1.060 (−1.235)	−84.12 (−94.17)
C_{48}–C_{49}	1.056 (1.400)	−1.110 (−1.340)	−87.16 (−104.89)
Mo–H_{61}	0.216 (0.027)	−0.151 (−0.022)	−46.15 (−8.03)
C_{58}–H_{61}	1.152 (0.937)	−0.605 (−0.732)	−65.09 (−91.67)

[a] The TAC model.
[b] Values in parentheses correspond to isolated systems ($Si_8O_{24}H_{16}$ and $Mo(C_3H_5)_4$).

formation of metal hydride is more feasible in this fixation model.

4.3. Electronic charge distribution

Table 3 displays net atomic charges in models TAC and TSC. Only the charges on the adsorbate and the active site atoms and its neighbors are presented. Several trends come out from the analysis of results shown in this Table

1. The exchange of a bidentate ligand on the surface for two allyls groups, as expected, leads to an electronic rearrangement in Mo and atoms bonded to it. For example, the most important changes for O atoms occur on those bonded to Mo (O_4 and O_{27}). Nevertheless, a comparison with the $Mo(C_3H_5)_4$ shows that the Mo atom is slightly less oxidized on the surface.
2. Population analysis for Si atoms in the cluster shows a large positive charge due to electronic transfer to oxygen atoms. The complex fixation affects the Si charge, specially those bonded to O atoms that are bonded to Mo. Charge on Si atoms decreases upon the anchoring of the complex.
3. The net electronic charge on C atoms of C_3H_5 ligands increases (about 0.35 a.u. with respect to the $Mo(C_3H_5)_4$ complex) after the anchoring on the surface.
4. Most of the H atoms of C_3H_5 ligands become more acidic (more positive charge on them), particularly H_{51}, H_{54}, H_{61} and H_{62}. This feature can also be used to explain the high activity of $Mo(C_3H_5)_2/SiO_2$ in the reaction of olefins metathesis. The acidic character of the allyl ligand protons found in this study may explain the enhancement of hydrogen mobility considered in the metathesis mechanism.
5. The total charge on O_4 and O_{27} decreases as two H atoms are substituted by $Mo(C_3H_5)_2$. It means that the complex fragment is a poorer electron donor than the two H atoms.
6. The Mo electronic charge decreases by the replacement of two C_3H_5 by the surface bidentate ligand. This fact may be due to the amount of electrons transferred to O ($q(O) = -0.77$ a.u.) from Si. It may affect the O capacity to store electronic charge. The Mo charge on TSC, TAC, and $Mo(C_3H_5)_4$ is different and depends on the kind of ligands associated with the Mo center. The charge is related with

Table 3
Net atomic charges of TSC and TAC models[a]

Atom	TSC	TAC
Si_1	+1.89 (+2.06)	+1.48 (+2.06)
O_2	−0.70 (−0.70)	−0.46 (−0.70)
O_4	−0.51 (−0.77)	−0.45 (−0.77)
O_5	−0.68 (−0.69)	−0.67 (−0.69)
O_7	−0.93 (−0.94)	−0.94 (−0.94)
Si_{22}	+1.73 (+1.95)	
O_{21}	−0.94 (−0.94)	
O_{23}	−0.67 (−0.68)	
O_{25}	−0.68 (−0.68)	
O_{27}	−0.53 (−0.68)	
Mo_{47}	+0.79 (+0.92)	+0.71
C_{48}	−0.20 (−0.09)	+0.11
C_{49}	+0.05 (−0.08)	−0.12
C_{50}	−0.11 (+0.01)	−0.27
H_{51}	+0.07 (+0.02)	+0.01
H_{52}	+0.03 (−0.00)	+0.07
H_{53}	+0.01 (−0.00)	+0.12
H_{54}	+0.05 (−0.03)	+0.07
H_{55}	−0.02 (−0.01)	+0.07
C_{56}	+0.00 (−0.08)	+0.08
C_{58}	−0.23 (−0.09)	−0.39
C_{59}	−0.19 (−0.02)	−0.23
H_{57}	−0.01 (+0.01)	−0.06
H_{60}	+0.01 (−0.01)	+0.06
H_{61}	+0.06 (−0.01)	+0.10
H_{62}	+0.06 (−0.01)	+0.03
H_{63}	−0.03 (−0.02)	+0.02

[a] Values in parentheses correspond to isolated systems ($Si_8O_{24}H_{16}$ and $Mo(C_3H_5)_4$).

the binding energy of the electrons. Thus, a major positive charge implies a higher binding energy. A variety of binding energies for Mo^{4+} systems have been reported from Mo 3d ESCA spectra [12].

7. The charge difference between $Mo(C_3H_5)_2$ on SiO_2 surface and in $Mo(C_3H_5)_4$ (0.35 a.u.) shows that there is an electronic drawing of electronic charge from the support to the complex fragment. This fact can be due to a stabilization of the electronic charge by delocalization in the π-cloud of allyl groups.

5. Conclusions

A modified CNDO-UHF method for calculating bonding energies is shown to be useful in complementing experimental studies for proposing anchored models of $Mo(\eta^3\text{-}C_3H_5)_2/SiO_2$. Calculations give support to the presence of η^3-allyl co-ordinated to Mo anchored on a silica surface. TSC (two separated centers) and TAC (two adjacent centers) sites in a silica are adequate for the formation of anchored $Mo(C_3H_5)_2$ species from the energetic point of view. In addition, several other interesting features can be drawn from this study

1. The formation of the anchored complex is preferred on a site located on oxygen atoms bonded to different Si atoms. TSC model is more stable than TAC one.
2. One of the allyl groups is bonded, besides to Mo, to an O atom on SiO_2. Therefore, there is a direct interaction of a allyl group with the support. This fact may be a fundamental issue regarding the catalytic metathesis mechanism, because a C–C bond in the allyl ligand is activated and allows the creation of an active site for further olefin adsorption.
3. There is C–H bond activation on the surface due to an important interaction between H and Mo. This fact supports the generally accepted mechanism of hydrogen transfer in olefin metathesis.
4. Small, but not negligible, bonding interactions between Mo–Si are observed.
5. A good correlation between the total energy balance and the total PDBE change of bonds involved in the complex-surface reaction shows that the anchoring process is mainly a local phenomenon.
6. Most of the H atoms of C_3H_5 ligands become more acidic (more positive charge on them). This feature can also be used to explain the activity of $Mo(C_3H_5)_2/SiO_2$ in the metathesis reaction of olefins.
7. Electronic charge transfer from the support to the π-cloud of $Mo(\eta^3\text{-}C_3H_5)_2$ complex is observed.

Acknowledgements

Support of this work by CONICIT through grant S1-2272 and G-9700667 gratefully acknowledged. We thank Susana Lobos for her assistance at the beginning of this work and Rafael Añez for calculation of MoSi.

References

[1] M. Che, D. Masure, P. Chaquin, J. Phys. Chem. 97 (1993) 9022.

[2] J.M. Basset, B.C. Gates, J.P. Candy, A. Chopin, M. Leconte, F. Quignard, C.C. Santini, Surface Organometallic Chemistry: Molecular Approaches to Surface Catalysis, Kluwer Academic Press, Dordrecht, 1988.
[3] J. Haber, in: H.F. Barry, P.C.H. Mitchell (Eds.), Climax Third International Conference on the Chemistry and Uses of Molybdenum, Climax Molybdenum Company, Ann Arbor, 1979, p. 114.
[4] J.P. Candlin, H. Thomas, in: D. Forster, J.F. Roth (Eds.), Homogeneous Catalysis, Vol. II, Ad. Chem. Series, 132 (1974) 212.
[5] J.L. Brito, B. Griffe, Catal. Lett. 50 (1998) 169.
[6] Yu.I. Yermakov, V. Zakharov, Adv. Catal. 24 (1975) 173.
[7] Yu.I. Yermakov, Catal. Rev. Sci. Eng. 13 (1976) 77.
[8] Y. Iwasawa, Adv. Catal. 35 (1987) 187.
[9] Y. Iwasawa, Catal. Today 18 (1993) 21.
[10] W.P. McKenna, E.M. Eyring, J. Mol. Catal. 29 (1985) 363.
[11] J.-J. Yu, M.Sc. Thesis, University of Pittsburgh, 1988.
[12] J.M. Aigler, J.L. Brito, P.A. Leach, M. Houalla, A. Proctor, N.J. Cooper, W.K. Hall, D.M. Hercules, J. Phys. Chem. 97 (1993) 5699.
[13] J.L. Brito, B. Griffe, M.J. Velásquez, S. Pekerar, in preparation.
[14] J.L. Brito, B. Griffe, S. Wolke, M.J. Velasquez, S. Pekerar, Extended Abstract, 11th I.C.C., Po-130, USA, 1996.
[15] M.J. Velásquez, M.Sc. Thesis, I.V.I.C., Caracas, Venezuela, 1996.
[16] J.A. Pople, D.L. Beveridge, Approximate Molecular Orbital Theory, McGraw-Hill, New York, 1970, p. 67.
[17] D. Rinaldi, GEOMO Program, QCPE, No. 290.
[18] A.J. Hernández, F. Ruette, E.V. Ludeña, J. Mol. Catal. 39 (1987) 21.
[19] F. Ruette, F.M. Poveda, A. Sierraalta, J. Rivero, Surf. Sci. 249 (1996) 241.
[20] F. Ruette, N. Valencia, R. Sánchez-Delgado, J. Am. Chem. Soc. 111 (1989) 40.
[21] A.E. Gainza, E.N. Rodríguez-Arias, F. Ruette, J. Mol. Catal. 85 (1993) 345.
[22] E.N. Rodríguez-Arias, A.E. Gainza, A.J. Hernández, P.S. Lobos, F. Ruette, J. Mol. Catal. 102 (1995) 163.
[23] Z. Benzo, W. Araujo, A. Sierraalta, F. Ruette, Anal. Chem. 65 (1993) 1107.
[24] A. Sierraalta, Z. Benzo, W. Araujo, F. Ruette, J. Mol. Struct. (Theochem.) 254 (1992) 387.
[25] R. Atencio, L. Rincón, R. Sánchez-Delgado, F. Ruette, Rev. Soc. Ven. Catál. 12 (1998) 28.
[26] H. Fisher, H. Kollmar, Theor. Chim. Acta 16 (1970) 163.
[27] M. Sanchez, F. Ruette, J. Mol. Struct. (Theochem.) 252 (1992) 335.
[28] A. Sierraalta, G. Frenking, Theor. Chim. Acta 95 (1997) 1.
[29] F. Ruette, G.L. Estiú, A.J. Jubert, R. Pis-Diez, Rev. Ven. Soc. Catal. 13 (1999) 57.
[30] A.W. Ehlers, G. Frenking, J. Chem. Soc., Chem. Commun., 1993, p. 1709.
[31] F.A. Cotton, G. Wilkinson, Advanced Inorganic Chemistry, Interscience New York, 3rd Edition, 1972, p. 113.
[32] Handbook of Chemistry and Physics, 53rd Edition, CRC Press, Cleveland OH, 1973, p. F-183.
[33] M.A. Tolbert, J.L. Beauchamp, J. Phys. Chem. 90 (1986) 5022.
[34] M.J. Frisch, G.W. Trucks, H.B. Schlegel, P.M.W. Gill, B.G. Johnson, M.A. Robb, J.R. Cheeseman, T. Keith, G.A. Peterson, J.A. Montgomery, K. Raghavachari, M.A. Al-Laham, V.G. Zakrzewski, J.V. Ortiz, J.B. Foresman, J. Cioslowski, B.B. Stefanov, A. Nanayakkara, M. Challacombe, C.Y. Peng, P.Y. Ayala, W. Chen, M.W. Wong, J.L. Andres, E. S Replogle, R. Gomperts, R.L. Martin, D.J. Fox, J.S. Binkley, D.J. Defrees, J. Baker, J.P. Stewart, M. Head-Gordon, C. Gonzalez, J.A. Pople, Gaussian 94, Revision D.4, Gaussian, Inc., Pittsburgh, PA, 1995.
[35] R.S. Mulliken, J. Chem. Phys. 23 (1955) 1841.
[36] M. Romero, M. Sánchez, A. Sierraalta, L. Rincón, F. Ruette, J. Chem. Infor. Comp. Sci. 39 (1999) 543.
[37] F. Ruette, C. González, A. Octavio, J. Mol. Struct. (Theochem.), in press.
[38] A. Szabo, N.S. Ostlund, in: Modern Quantum Chemistry: Introduction to Advanced Electronic Structure Theory, MacMillan, New York, 1982, p. 151, 173.
[39] T.B. Shay, L.Y. Hsu, J.M. Basset, G.S. Shore, J. Mol. Catal. 86 (1994) 479.
[40] L.T. Zhuralev, Langmuir 3 (1987) 316.
[41] P. Van Der Voort, I. Gillis-D'Hammers, K.C. Vrancken, E.F. Vasant, J. Chem. Soc., Faraday Trans. 87 (1991) 3899.
[42] R. Benn, S. Holle, P.W. Jolly, C. Krüger, C.C. Romão, M.J. Romão, A. Rufinska, G. Schroth, Polyhedron 5 (1986) 461.
[43] K.C. Ramey, D.C. Lini, W.B. Wise, J. Am. Chem. Soc. 90 (1968) 4275.
[44] T.R. Welberry, G.L. Hua, R.L. Withers, J. Appl. Crystallogr. 22 (1989) 87.
[45] F. Vigne-Maeder, P. Sautet, J. Phys. Chem. B 101 (1997) 8197.
[46] B. Civalleri, S. Casassa, E. Garone, C. Pisani, P. Ugliengo, J. Phys. Chem. B 103 (1999) 2165.
[47] Y. Iwasawa, H. Kubo, H. Hamamura, J. Mol. Catal. 28 (1985) 191.